Pesticide Biochemistry and Physiology 213 (2025) 106520

Contents lists available at ScienceDirect

Pesticide Biochemistry and Physiology

journal homepage: www.elsevier.com/locate/pest

# Sublethal effects of dimethoate on energy metabolism and its link to cellular senescence due to impaired mitochondrial respiration and ATP production in SH-SY5Y cells

Phorutai Pearngam [a], Kornkanok Promthep [b], Tanya Prasertporn [b], Kittikun Songsomboon [c], Tanthai Polvat [b], Jiratchaya Charoenkul [a], Sujira Mukda [b], Piyarat Govitrapong [d], Chutikorn Nopparat [e,*], Jiraporn Panmanee [b,*]

[a] Biological Sciences Program, Mahidol University International College, Mahidol University, Nakhon Pathom 73170, Thailand
[b] Research Center for Neuroscience, Institute of Molecular Biosciences, Mahidol University, Nakhon Pathom 73170, Thailand
[c] Climate Change Cluster, University of Technology Sydney, Ultimo, Sydney, NSW 2007, Australia
[d] Chulabhorn Graduate Institute, Laksi, Bangkok, Thailand
[e] Innovative Learning Center, Srinakharinwirot University, Sukhumvit 23, Bangkok 10110, Thailand

ARTICLE INFO

*Keywords:*
Dimethoate
Pesticide
Neurotoxicity
Mitochondria
Senescence

Abstract

Dimethoate (DM), a widely used organophosphate pesticide, induces significant alterations in mitochondrial-related proteomes of SH-SY5Y cells without directly affecting cell viability. After, cells were exposed to 100 μM DM for 48 h, proteomic analysis revealed that 27 proteins associated with cellular metabolism and mitochondrial function were notably altered, affecting pathways such as oxidative phosphorylation, electron transport chain, and ATP synthesis. At sublethal concentrations, DM reduced mitochondrial ATP production, oxygen consumption rates (OCR), basal and maximal respiration, while preserving spare respiratory capacity (SRC) and proton leak, indicating maintained mitochondrial membrane integrity. Despite this, DM exposure caused mitochondrial membrane depolarization and increased mitochondrial superoxide production. These mitochondrial alterations were accompanied by enhanced cellular senescence, marked by p53-independent p21 activation, p38 MAPK activation, increased senescence-associated β-galactosidase (SA-β-gal) activity, and disrupted cell cycle progression. Additionally, DM treatment led to upregulation of DNA damage response (DDR) proteins and downregulation of proteins involved in DNA repair and genome stability. Although early-stage apoptosis was observed, elevated Bcl-2 expression suggested a shift toward apoptosis resistance and senescence. DM also disrupted energy-sensing pathways by increasing AMPK subunit expression, yet suppressed autophagy, as indicated by decreased p-mTOR, p-Beclin-1, and LC3-II/I ratios. Collectively, these findings highlight a complex interplay between mitochondrial dysfunction, cellular senescence, and survival mechanisms, suggesting potential long-term effects of DM exposure on cellular health and aging processes.

*Abbreviations:* ASH1L, ASH1 Like Histone Lysine Methyltransferase; BECN1, Beclin-1; BRCA1, Breast Cancer Type 1 Susceptibility Protein; CBX8, Chromobox 8; CDK13, Cyclin-Dependent Kinase 13; COX6A1, Cytochrome c Oxidase Subunit 6A1; CYCS, Cytochrome c, Somatic; DDIAS, DNA Damage Induced Apoptosis Suppressor; DHX9, DEAH-box Helicase 9; DNMT1, DNA Methyltransferase 1; EHMT1, Euchromatic Histone Lysine Methyltransferase 1; EZH2, Histone-lysine *N*-methyltransferase EZH2; GFM2, G Elongation Factor Mitochondrial 2; GLDC, Glycine Decarboxylase; HSF1, Heat Shock Factor 1; INO80, Chromatin-remodeling ATPase INO80; ISCA1, Iron-Sulfur Cluster Assembly 1; KMT2D, Lysine Methyltransferase 2D; KMT2E, Lysine Methyltransferase 2E; MIEF2, Mitochondrial Elongation Factor 2; MRPL2, Mitochondrial Ribosomal Protein L2; MRPL22, Mitochondrial Ribosomal Protein L22; mtATP6, Mitochondrially Encoded ATP Synthase Membrane Subunit 6; MTIF2, Mitochondrial Translation Initiation Factor 2; MTO1, Mitochondrial tRNA Translation Optimization 1; MTOR, Mechanistic target of rapamycin; NDUFS2, NADH Oxidoreductase Core Subunit S2; NDUFS7, NADH Oxidoreductase Core Subunit S7; PKMYT1, Protein Kinase, Membrane Associated Tyrosine/Threonine 1,; POLQ, DNA Polymerase Theta; POLRMT, RNA Polymerase Mitochondrial; PRKAB1, AMP-activated protein kinase subunit beta-1; RHEB, Ras homolog enriched in brain; RPTOR, Regulatory associated protein of mTOR; SIRT1, Sirtuin 1; SMCHD1, Structural Maintenance of Chromosomes Flexible Hinge Domain Containing 1; TIMM44, Translocase of Inner Mitochondrial Membrane 44; TK2, Thymidine Kinase 2; TRNT1, tRNA Nucleotidyl Transferase 1..

* Corresponding authors.
*E-mail addresses:* chutikorn@g.swu.ac.th (C. Nopparat), jiraporn.pam@mahidol.edu, jiraporn.pam@mahidol.ac.th (J. Panmanee).

https://doi.org/10.1016/j.pestbp.2025.106520
Received 27 February 2025; Received in revised form 16 June 2025; Accepted 20 June 2025
Available online 20 June 2025

## 1. Introduction

Dimethoate (DM) is one of the most commonly used pesticide worldwide in agriculture and livestock industries. It belongs to the organophosphate class, and its primary mode of action involves forming covalent bonds with the acetylcholinesterase (AChE), an enzyme playing a key role in the cholinergic signaling (Fukuto, 1990). DM possesses neurotoxic properties and has detrimental effects on other systems, such as the reproductive and immune systems, posing potential health risks for humans, livestock and off-target animals (Aly, 2000; Kim and Kang, 2015; Tarbah et al., 2007; Van Scoy et al., 2016; Walsh et al., 2000). The residual pesticides were detected in fruits, vegetable, and drinking water (Sagar et al., 2018; Sang et al., 2022). Approximately 14 % of DM can be absorbed through the human skin, posing a risk of chronic exposure for farm workers (de Andrade et al., 2022). Following exposure, DM can enter the bloodstream and affect various organs, including the brain (Tarbah et al., 2007).

The recent study found that DM treatments triggered the release of intracellular $Ca^{2+}$ store and increased reactive oxygen species (ROS) generation in the mitochondria of rat brain, liver and pancreatic stellate cells (Martínez-Morcillo et al., 2019; Sharma et al., 2005). Sub-chronic exposure of DM at 1.4 mg/kg for five weeks resulted in an increase expression of the pro-inflammatory markers and microglia reactivation in mouse hippocampus and striatum (Astiz et al., 2013). Recently, a study showed that DM at 125–500 μM can directly interact with the Nod-like receptor with the $K_D$ of 89.8 μM and increased the expression of IL-1β and IL-18 in BV2 microglial cells (Wang et al., 2024). Furthermore, prolonged exposure to low levels of DM resulted in cellular oxidative stress, DNA damage and disrupted membrane-integrated ATPases in visceral organs (Ben Amara et al., 2013). Moreover, the study on the acute toxicity of DM in rat leukocytes revealed that various doses of DM (20–60 mg/kg) led to a reduction in mitochondrial membrane potential (MMP), disruption in cell cycle, and cellular apoptosis (Nazam et al., 2020).

However, little is known about the direct effect of DM on neuronal energy metabolism and ATP production. Previous research has established that mitochondrial dysfunction and cellular senescence are the hallmarks of aging (Correia-Melo et al., 2016; Miwa et al., 2022), indicating a potential connection between these metabolic changes and the cellular processes influenced by toxic exposures. Considering the widespread application of organophosphates and their associated risks, a thorough examination of these compounds regarding their spectrum of toxicity in neuronal models is important. In this study, we aim to examine the relationship between impaired energy metabolism, cellular senescence, and cellular apoptosis in DM exposure at a sublethal concentration.

## 2. Materials and methods

### 2.1. Chemical and reagents

The chemicals used in this research were obtained from various manufacturers as follows: Dulbecco's Modified Eagle Medium (DMEM)/Nutrient Mixture F-12 and phosphate-buffered saline (PBS) from Sartorius; fetal bovine serum (FBS) from Biological Industries; dimethyl sulfoxide (DMSO), dithiothreitol (DTT), MTT (3-(4,5-dimethylthiazol-2-yl)-2,5-diphenyltetrazolium bromide), and the senescence cell histochemical staining kit from Sigma-Aldrich; cypermethrin and dimethoate from Dr. Ehrenstorfer™; propidium iodide from Abcam; Bradford reagent from Bio-Rad; MitoSOX™ Red from Invitrogen; Muse® Annexin V & Dead Cell Kit and Muse® MitoPotential Kit from Luminex; Seahorse XF Cell Mito Stress Test kit from Agilent. Primary antibodies from Cell Signaling Technology included rabbit anti-p21 (#2947), rabbit anti-p53 (#9282), mouse anti-Bcl-2 (#15071), rabbit anti-phospho-p38 MAPK (Thr180/Tyr182) (#4511), rabbit anti-p38 MAPK (#8690), rabbit anti-phospho-AMPKα (Thr172) (40H9) (#2535), rabbit anti-AMPKα (D5A2) (#5831), rabbit anti-Bax (#2772), rabbit anti-Beclin-1 (D40C5) (#3495), rabbit anti-phospho-Beclin-1 (Ser30) (E1C4X) (#35955), rabbit anti-Cleaved Caspase-3 (Asp175) (5A1E) (#9664), rabbit anti-LC3B (#2775), rabbit anti-mTOR (7C10) (#2983), rabbit anti-phospho-mTOR (Ser2448) (D9C2) XP® (#5536), and mouse anti-beta-actin (#3700), and HRP (horseradish peroxidase)-conjugated anti-mouse and anti-rabbit secondary antibodies.

### 2.2. Cellular treatments

Human neuroblastoma SH-SY5Y cells were cultured in DMEM/F-12 medium (1:1 ratio), supplemented with 10 % FBS, in a humidified atmosphere with 5 % $CO_2$ at 37 °C. Cells were seeded at a density of $3 \times 10^5$ cells per well in 6-well plates and allowed to adhere overnight. To evaluate the neurotoxic effects of DM, cells were treated with 100 μM DM in serum-free medium for 24 or 48 h. After treatment, cells were collected and used for subsequent experiments. For comparison, some experiments included treatment with cypermethrin (CYP) under identical conditions as the DM treatments. Stock solutions of DM and CYP were prepared in 100 % DMSO. The final concentration of DMSO were less than 0.1 % in all experiments.

### 2.3. MTT assay for detection of cell metabolic state

Cells were seeded in 96-well plates at a density of $1 \times 10^4$ cells per well and allowed to grow overnight at 37 °C in an atmosphere of 5 % $CO_2$. Final concentrations of 25, 50, and 100 μM of DM were administered, and cells were incubated for 24 or 48 h. For the MTT assay, 100 μL of serum-free medium containing MTT at a concentration of 0.5 mg/mL was added to each well, followed by a 4-h incubation at 37 °C with 5 % $CO_2$. Then, the MTT solution was removed from the wells, formazan crystals produced by living cells were dissolved by 100 μL DMSO. The reaction was agitated at 37 °C for 15 min. Measurement of absorbance at 570 nm was carried out using a microplate reader (EZ Read 2000, Biochrom).

### 2.4. Cell viability assessment

Cells were harvested and resuspended in the culture medium at an appropriate density ($5 \times 10^5$ cells/mL). For viability assessment, 10 μL of the cell suspension was mixed with 10 μL of 0.4 % trypan blue solution (Bio-Rad, Cat# 1450021) in a 1:1 ratio. After thorough mixing, 10 μL of the mixture was loaded into a TC10™ counting slide (Bio-Rad, Cat# 1450010), and measurements were performed using the TC10™ Automated Cell Counter (Bio-Rad Laboratories, USA) following the manufacturer's instructions. Total cell number, live cell count, and viability percentage (% viable cells) were recorded. Cell viability was calculated as the percentage of live cells relative to the total number of cells.

### 2.5. Label-free nano-LC-MS/MS analysis for proteomics study

Untargeted label-free nano-LC-MS/MS and SWATH targeted label-free Nano-LC QTOF analyses were carried out following the previously described protocol by (Na Nakorn et al., 2020). For protein identification during the discovery phase, raw mass spectrometry (MS) data were processed using MaxQuant software (version 1.6.2.10) with the integrated Andromeda search engine. The human protein database from UniProt was used, and a label-free quantification method was applied with a default setting of 1. All parameters were set to default except for the following modifications: methionine oxidation and N-terminal acetylation were treated as variable modifications, while cysteine carbamidomethylation was applied as a fixed modification. The Bruker Q-TOF mass spectrometer was selected, with peptide mass tolerances set to 0.5 Da for the initial search and 0.25 Da for the major search. Trypsin/P enzyme was used, allowing up to two missed cleavages for peptide

identification. Label-free quantification (LFQ) required a minimum ratio count of 1. The raw data were matched against the UniProt database for *Homo sapiens*, with a false discovery rate (FDR) of 1 % at the protein level. For LFQ, the MS/MS match tolerance was also set to 0.5 Da, and the "match between runs" feature was enabled to adjust mass and retention times across different runs. In total, 1665 proteins were identified, the differentially expressed proteins were determined by the unpaired *t*-test with a significant level at 0.05 (see Statistical analysis). the The proteins of interest were further analyzed for protein-protein interactions and pathways using the STRING database (www.string-db.org). The Gene Ontology (GO term) was used to classify pathways and proteins of interest. The GOnet (https://tools.dice-database.org/GOnet/) was used to visualize enriched related pathways and proteins of interest (Pomaznoy et al., 2018).

### 2.6. Cellular respiration assay

Oxygen consumption rate (OCR), a key indicator of cellular respiration, was detected using the XF96 Extracellular Flux Analyzer (Seahorse Bioscience, Billerica, MA, USA). SH-SY5Y cells were plated at $1 \times 10^4$ cells per well. 180 μL of bicarbonate-free DMEM containing 10 mM glucose, 2 mM L-glutamine, and 1 mM sodium pyruvate were added and incubated for 45 min at 37 °C. Mitochondrial function were measured utilizing mitochondrial inhibitors and uncouplers using XF Cell Mito Stress Test (Seahorse Bioscience). Sequential injections included 1 μM oligomycin to block ATP synthase activity, 0.5 μM FCCP to induce maximal respiration, and rotenone and antimycin A mixture at the final concentration of 1 μM each to block electron transport at complexes I and III. Baseline OCR was recorded before treatment, followed by measurements after each injection to assess specific respiratory parameters including ATP-associated respiration, maximal respiratory capacity, and spare capacity. Total protein concentrations, used for data normalization, was quantified using the Bradford assay (Bio-Rad).

### 2.7. Senescence-associated β-galactosidase detection

Cellular senescence was assessed using a senescence-associated β-galactosidase (SA-β-gal) staining kit as described by (Promthep et al., 2022). Briefly, cells were first rinsed with PBS and fixed in a 1× fixative solution for 7 min. After another PBS wash, freshly prepared SA-β-gal staining solution was added. The parafilm-sealed plate was incubated at 37 °C for 15 h without $CO_2$. Blue-stained cells indicating SA-β-gal activity were examined under a light microscope. SA-β-gal-positive cells were counted and quantified as a percentage in three randomly selected fields and compared with untreated controls.

### 2.8. Cell cycle distribution analysis

Cell cycle distribution was analyzed using a modified propidium iodide (PI) staining protocol described by (Zhou et al., 2015). The cells were first trypsinized, washed with ice-cold PBS, and then spun down to collect the pellets. These pellets were resuspended in PBS and fixed with 70 % ethanol at 4 °C for 1 h. After fixation, the cells were washed again with PBS and stained with 40 μg/mL propidium iodide (PI) and 40 μg/mL RNase I for 30 min at room temperature. The cell cycle distribution was analyzed using a BD FACSCanto™ flow cytometer (BD Biosciences, USA), and the data were evaluated with FACSDiva software (Version 6.1.1). A total of 30,000 events were acquired for each sample.

### 2.9. Cellular apoptotic assay

The apoptotic response in SH-SY5Y cells treated with CYP and DM was assessed using the Muse™ Annexin-V & Dead Cell Assay Kit (Luminex, Austin, TX, USA), following the manufacturer's guidelines. SH-SY5Y cells were seeded into 6-well plates at a density of $2.5 \times 10^5$ cells per well and cultured overnight. Following incubation, the cells were exposed to 100 μM of either CYP or DM for 48 h under standard conditions (37 °C, 5 % $CO_2$). After treatment, cells were collected and washed with cold PBS. Cells were spun down at 1000 rpm for 5 min and resuspended in serum-free medium. 100 μL Muse™ Annexin-V & Dead Cell Reagent was used to stain cell suspensions with 100 μL Muse™ Annexin-V & Dead Cell Reagent, and cells were protected from light and maintained for 20 min at room temperature. Live, early apoptotic, late apoptotic, and necrotic cells, were measured using the Muse™ Cell Analyzer (Luminex, Austin, TX, USA).

### 2.10. Western blotting

For protein extraction, SH-SY5Y cells were lysed using RIPA buffer containing 50 mM Tris base, 1 m PMSF, 1 mM EDTA, 150 mM NaCl, 0.1 % Triton X-100, protease inhibitors, phosphatase inhibitors, and SDS. After sonication, the lysate was spun down at 12,000 ×*g* for 15 min at 4 °C. The total protein concentration was measured using the Bradford reagent. Protein samples (40–50 μg) were mixed with sample loading buffer, separated by 10–12 % SDS-PAGE at 120 V, and transferred to PVDF membranes at 100 V for 3 h. The membranes were blocked with 5 % nonfat milk in TBST for 1 h at room temperature. Subsequently, they were incubated overnight at 4 °C with primary antibodies at the following dilutions: 1:1000 for p21, p53, phospho-p38 MAPK, p38 MAPK, and Bcl-2; 1:500 for Bax, LC3B, cleaved-caspase 3, p-mTOR, mTOR, p-beclin-1, beclin-1, AMPK, p-AMPK; and 1:5000 for β-actin. After primary antibody incubation, HRP-conjugated secondary antibodies were further incubated for 1.5 h at room temperature. Chemiluminescent detection was performed using Clarity Western ECL Substrate (Bio-Rad), and signals were captured with the Fusion FX7 Image Analyzer (Vilber). The intensity of protein band was quantified using ImageJ software, with β-actin used as the loading control for normalization.

### 2.11. Mitochondrial ROS detection

Mitochondrial superoxide levels were assessed using MitoSOX™ Red (Invitrogen) as previously described by (Panmanee et al., 2025). SH-SY5Y cells were seeded in 96-well PhenoPlates™ and treated with 100 μM DM for 24 h and 48 h, respectively. Imaging was performed using the Opera Phenix Plus high-content screening system (PerkinElmer) witg 561 nm excitation, and 570–630 nm emission, and a 40× objective, capturing 25 fields per well. Image analysis of fluorescence intensity was performed using Harmony software (PerkinElmer) to evaluate mitochondrial ROS levels.

### 2.12. Measurement of mitochondrial membrane potential

Mitochondrial membrane potential (Δψm) was evaluated using the Muse® MitoPotential Kit (Luminex) according to the manufacturer's protocol. Briefly, SH-SY5Y cells were seeded in 6-well plates and treated with 100 μM DM for 48 h. After treatment, cells were harvested by trypsinization, washed with 1× PBS, and resuspended in assay buffer. Approximately $1 \times 10^5$ cells/mL were incubated with the MitoPotential Dye for 20 min at 37 °C in the dark, followed by addition of 7-Aminoactinomycin D (7-AAD) to discriminate dead cells. The stained samples were analyzed using the Muse® Cell Analyzer. Data were expressed as the percentage of cells with depolarized mitochondria among the total and viable cell populations. At least 2000 events were collected per sample, and data analysis was conducted using Muse® Analysis Software.

### 2.13. Statistical analysis

The untreated control group was compared to the DM-treated group using an unpaired *t*-test. For comparisons involving more than two treatment groups, statistical analysis was conducted using one-way

ANOVA followed by Tukey's post hoc test. Data were considered significant when *P*-values <0.05. Data are expressed as the mean ± standard error of the mean (SEM). All experiments were carried out independently, with at least three replicates.

In untargeted label-free nano-LC-MS/MS proteomics study, the differentially expressed proteins were determined by the unpaired t-test with a significant level at 0.05. For the SWATH targeted label-free analysis, data processing and statistical analysis were performed in R (version 4.4.1) (R.C. Team, 2014). The raw SWATH-MS data was calculated into total area sums, log2-transformed, and loess normalization via limma package (Ritchie et al., 2015). The normalized log2 total area was fitted to linear models for each protein using the lm function and post-hoc pairwise comparisons adjusting for multiple comparisons using Tukey's method via emmean package (Russell, 2018). The custom R script is available at https://github.com/skittikun/SWATH_Dimethoate.

## 3. Results

### 3.1. DM treatment did not directly affect cell viability but changed the mitochondrial-related proteomes of SH-SY5Y cells

To assess cell viability after exposure to various concentrations of DM in SH-SY5Y cells, DM at 25, 50, and 100 μM was administered and incubated for 24 and 48 h, respectively. Mitochondrial metabolic activity was assessed using the MTT assay, while total cell number and viability were independently confirmed using the TC10™ Automated Cell Counter. The results showed that cells treated with DM for 24 h and 48 h exhibited a metabolic activity and cell viability comparable to the control (Figs. 1A, B, and C). Therefore, to examine the neurotoxic effect of DM, the prolonged treatment at 48 h of 100 μM DM was selected for subsequent experiments.

To test the proteomics profiles of cells exposed to the pesticide, DM-treated cells were analyzed using untargeted label-free LC-MS/MS. A total of forty-five proteins were found to be differentially expressed related to functional mitochondrial organization, cellular senescence, DNA damage repair, and cell cycle regulators in DM-exposed cells (Fig. 2A). Among these, twenty-seven proteins related to cellular metabolism and mitochondrial function were significantly altered by DM treatment (Fig. 2B). Key pathways affected include oxidative phosphorylation (GO:0006119), electron transport chain (GO:0022900), and ATP metabolic processes (GO:0046034). Proteins such as CYCS, COX6A1, POLRMT, FECH, GLDC, ISCA1, MIEF2, TIMM44, NDUFS2 and NDUFS7 are involved in mitochondrial organization and energy generation (Figs. 2B and C). Additionally, changes were observed in proteins related to mitochondrial gene expression (GO:0140053), including TRNT1, MTO1, GFM2, MTIF2, MRPL2, and MRPL22, suggesting possible disturbances in mitochondrial transcription and translation. Based on these alterations, DM exposure could result in broader metabolic dysfunction within the cell.

### 3.2. DM at sublethal concentration reduced mitochondrial ATP production in SH-SY5Y cells

The changes identified by proteomics studies indicated that DM altered several proteins associated with mitochondrial function (Figs. 2A, B and C). We hypothesized that DM likely disrupted ATP synthesis and overall cellular energy homeostasis. To test this hypothesis, energy metabolism during oxidative phosphorylation in cells exposed to 100 μM DM for 48 h was assessed using a fluorescence-based Seahorse XF analyzer. DM treatment led to decrease in oxygen consumption rates (OCR), basal respiration, maximal respiration, and ATP production (Figs. 3A, B, C, and D). However, the spare respiratory capacity (SRC) and proton leak were unaffected by DM treatment (Figs. 3E and F), suggesting that while mitochondrial bioenergetic function was impaired, the integrity of the inner mitochondrial membrane was

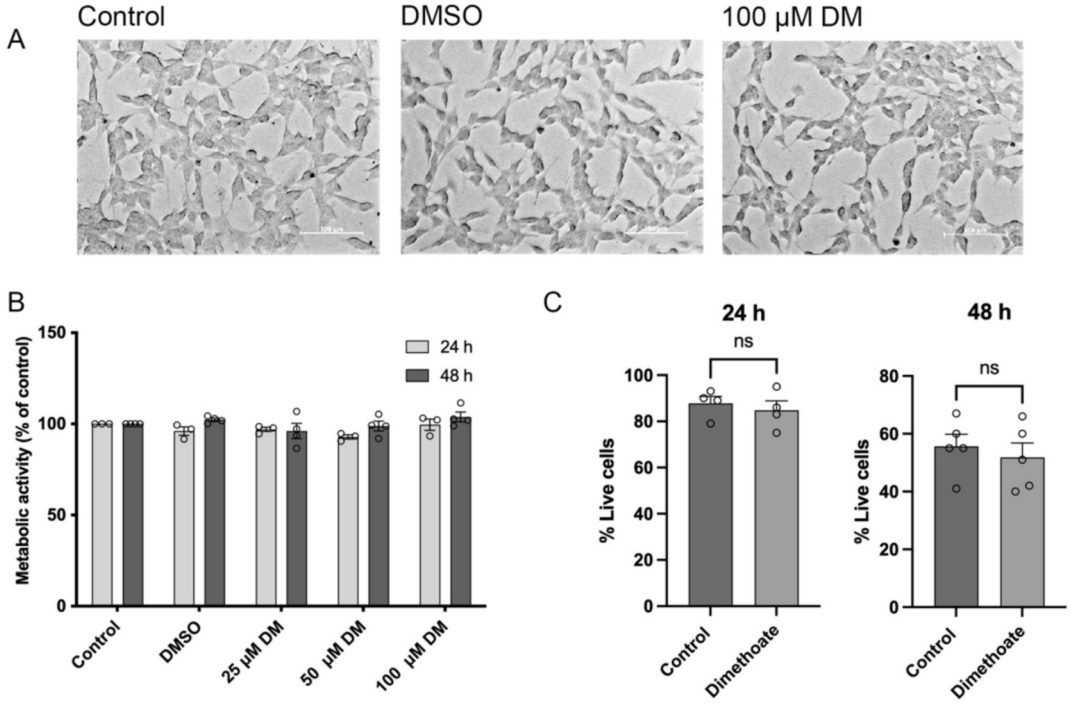


**Fig. 1.** Effect of pesticide exposure on cell morphology, metabolic activity, and cell viability. **(A)** Representative images of SH-SY5Y cells after 48 h of incubation with 0 μM DM (control), 0.1 % DMSO, and 100 μM DM, respectively. Scale bars: 100 μm. **(B)** MTT assay was assessed to evaluate cellular metabolic activity in SH-SY5Y cells treated with DM at 25, 50, and 100 μM for 24 h and 48 h. **(C)** Live cell count of SH-SY5Y cells treated with 100 μM DM for 24 and 48 h, measured using the TC10™ Automated Cell Counter. Cell viability was assessed based on membrane integrity using trypan blue. Live cell numbers are presented as a proportion of the total cell count. The data represent the mean ± SEM ($n = 3$–5). (For interpretation of the references to colour in this figure legend, the reader is referred to the web version of this article.)

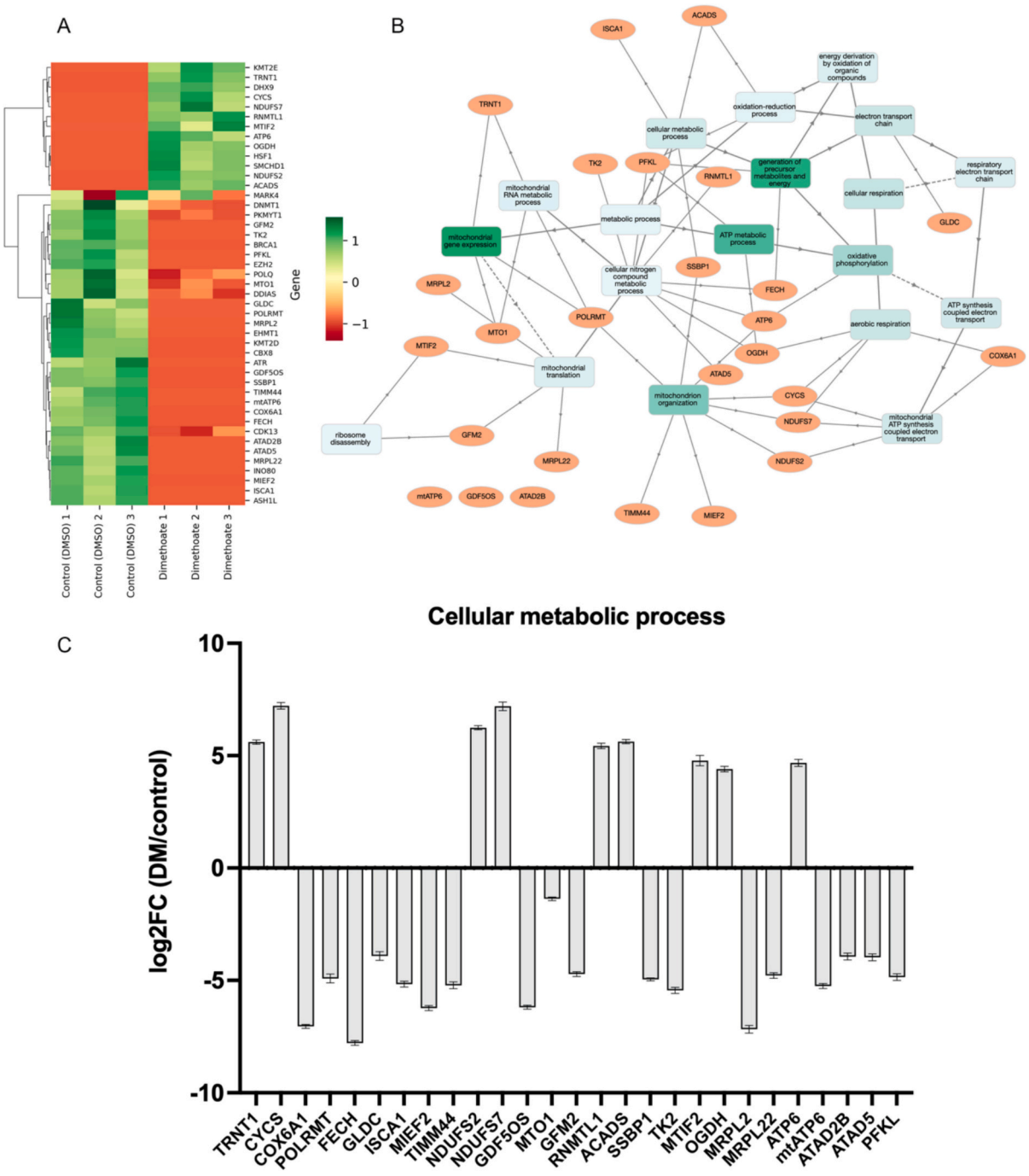


**Fig. 2.** Effect of DM treatment on mitochondrial function and cellular metabolic process. **(A)** The heatmap illustrates the expression levels of 45 proteins in both control and DM-treated cells, clustered based on clustered based on z-score-normalized individual label-free quantitation (LFQ) values from three independent experiments. **(B)** GO enrichment network of genes significantly altered following 48-h DM treatment was constructed using GOnet. In the network, orange ellipses indicate genes identified from the dataset, and green rectangles represent GO terms that are significantly enriched. Interaction network and GO term analysis of mitochondrial protein are shown as follows; electron transport chain (GO:0022900), mitochondrial ATP synthesis coupled electron transport (GO:0042775), mitochondrial gene expression (GO:0140053), oxidative phosphorylation (GO:0006119), metabolic process (GO:0046034), metabolic process (GO:0008152), mitochondrial gene expression (GO:0140053), generation of precursor metabolites and energy (GO:0006091), and cellular metabolic process (GO:0044237). **(C)** Differential protein expression levels ($log_2FC$), calculated from the label-free quantitation (LFQ) values from three independent experiments, in DM-treated cells compared to the untreated control are shown. (For interpretation of the references to colour in this figure legend, the reader is referred to the web version of this article.)

largely preserved.

Despite the maintained membrane integrity, mitochondrial membrane potential was significantly depolarized in cells treated with DM for 48 h (Figs. 3G and H). Additionally, MitoSOX™ Red staining revealed a marked increase in mitochondrial superoxide production both 24-h and 48-h DM-exposed cells, indicating elevated oxidative stress within the mitochondria (Figs. 3I and J).

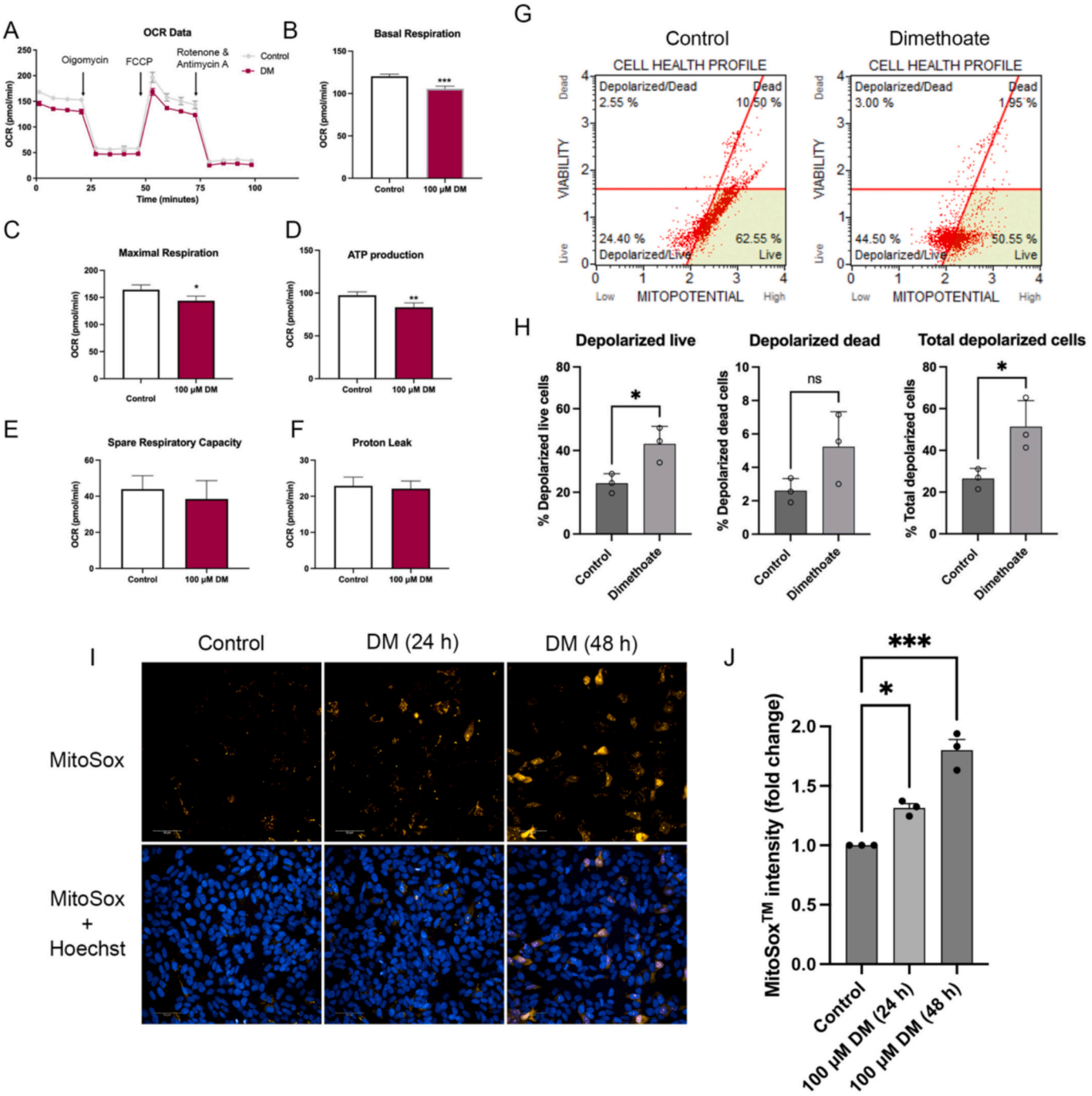


**Fig. 3.** Effect of dimethoate on ATP production and mitochondrial membrane potential. Mitochondrial respiration function parameters of SH-SY5Y cells exposed to DM were assessed using the Seahorse XFe96 extracellular flux analyzer. **(A)** The oxygen consumption rate (OCR) changes are illustrated. **(B—F)** Bar charts display mitochondrial respiration changes in DM-treated cells, including basal respiration (B), maximal respiration (C), ATP production (D), spare respiratory capacity (E), and proton leak (F). **(G–H)** Mitochondrial membrane depolarization was analyzed using the Muse® MitoPotential Kit. **(G)** Representative profiles show depolarized live/dead cells, live cells, and dead cells. **(H)** Bar charts present the percentages of live, dead, and total depolarized cells. **(I)** Representative fluorescent images of control and DM-treated cells at 24 and 48 h are shown. **(J)** Quantification of MitoSOX™ fluorescence intensity is presented for each condition, exhibiting mitochondrial superoxide levels. Data represent the mean ± SEM ($n = 3$–4). Significant differences are denoted as $^{*}p < 0.05$, $^{**}p < 0.01$, $^{***}p < 0.001$.

### *3.3. DM exposure increased senescence-related protein expression and disrupted cell cycle process*

Impaired energy metabolism is known to be associated with cellular senescence and aging since mitochondrial respiration and ATP production decrease with age (Miwa et al., 2022; Wiley and Campisi, 2021). The cellular senescence markers were, thus, assessed in cells exposed to 100 μM DM for 48 h.

Under the treatment of DM at 100 μM for 48 h, a substantial expression of p21, a cellular senescence marker, was detected, with a notable decrease in expression of p53 (Fig. 4A). The result suggests that DM exposure induced p53-independent activation of p21. DM also elevated the activation of p38 mitogen-activated protein kinase (MAPK) involving in the apoptotic and senescence-signaling pathway (Fig. 4A). To further investigate the effect of DM on cellular senescence, SA-β-gal was used as a marker of senescence-like activity (Fig. 4B). The findings

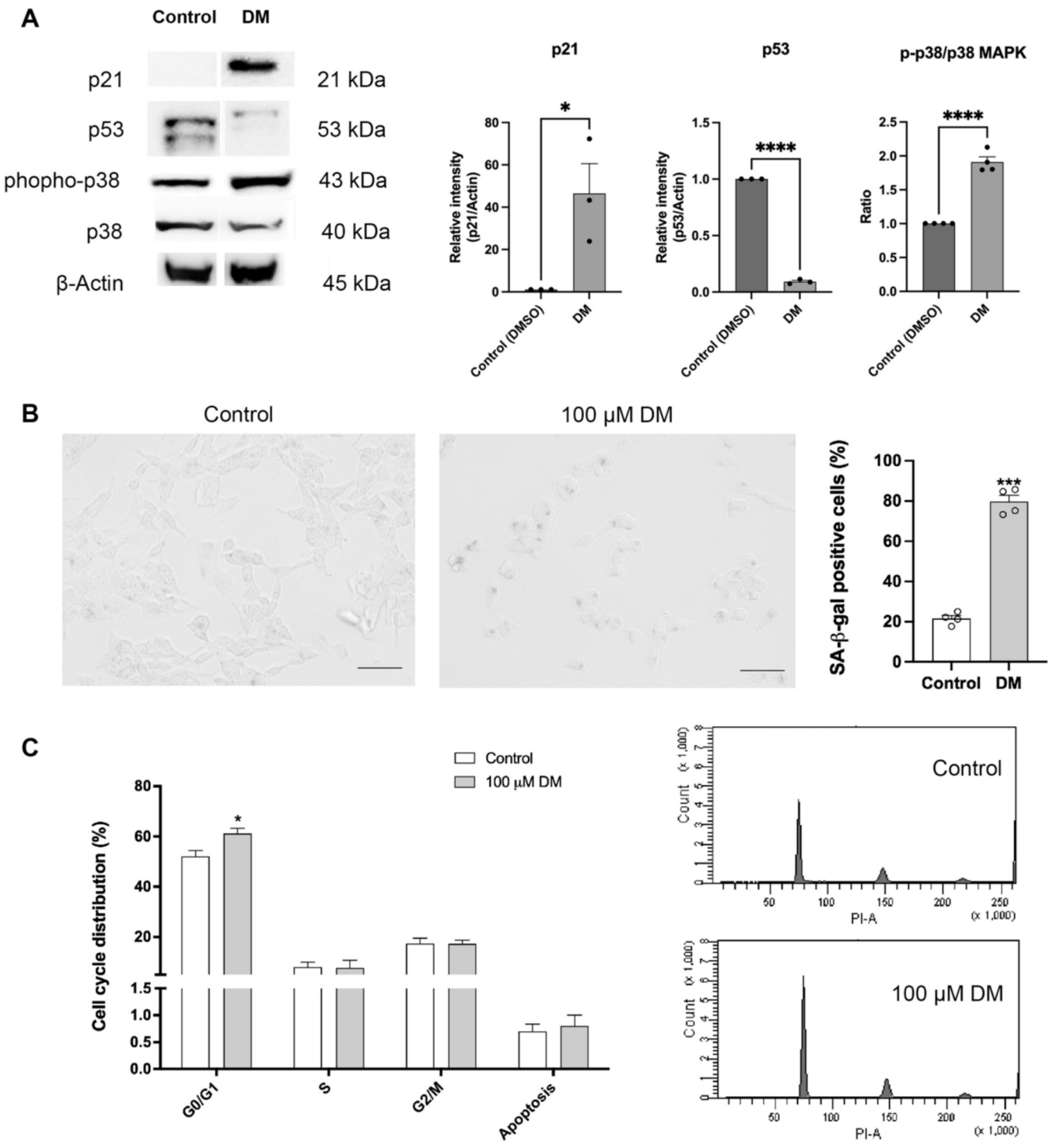


**Fig. 4.** Effects of DM exposure on cell cycle regulation and markers associated cellular senescence. **(A)** Effects of DM exposure for 48 h on p21, p53 and p-p38/ p38 MAPK protein expressions were analyzed by Western blot. **(B)** SA-β-gal staining was carried out to detect senescent cells, comparing untreated controls with those treated with 100 μM DM for 48 h. The percentage of SA-β-gal-positive cells was quantified and compared to untreated controls. Scale bars: 100 μm. **(C)** Flow cytometry was employed for cell cycle analysis. Data are presented as mean ± SEM ($n = 3$–4), and significance is denoted as $^{*}p < 0.05$, $^{**}p < 0.01$, $^{***}p < 0.001$, and $^{****}p < 0.0001$ compared to the control group.

indicated that DM treatment significantly enhanced SA-β-gal activity compared to the untreated cells ($p < 0.001$). Moreover, cell cycle analysis revealed an increase in cells during the $G_0/G_1$ phase after DM treatment ($p < 0.05$), representing cell cycle arrest (Fig. 4C). Cell cycle regulators such as CDK13 ($log_2FC$, −1.4) were downregulated by DM treatment (Fig. 5). Notably, DM exposure led to the upregulation of proteins that inhibit cell cycle progression such as KMT2E ($log_2FC$, 4.89), but downregulated several proteins involved in promoting cell cycle progression including KMT2D ($log_2FC$, −2.53), EHMT1 ($log_2FC$, −5.29), EZH2 ($log_2FC$, −5.20), ASH1L ($log_2FC$, −4.18), DNMT1 ($log_2FC$, −1.27), INO80 ($log_2FC$, −5.23) and PKMYT1 ($log_2FC$, −2.24) (Figs. 5A and B). The results indicated that DM treatment potentially accelerated senescence-related changes, further supporting the link between impaired mitochondrial function, reduced energy metabolism,

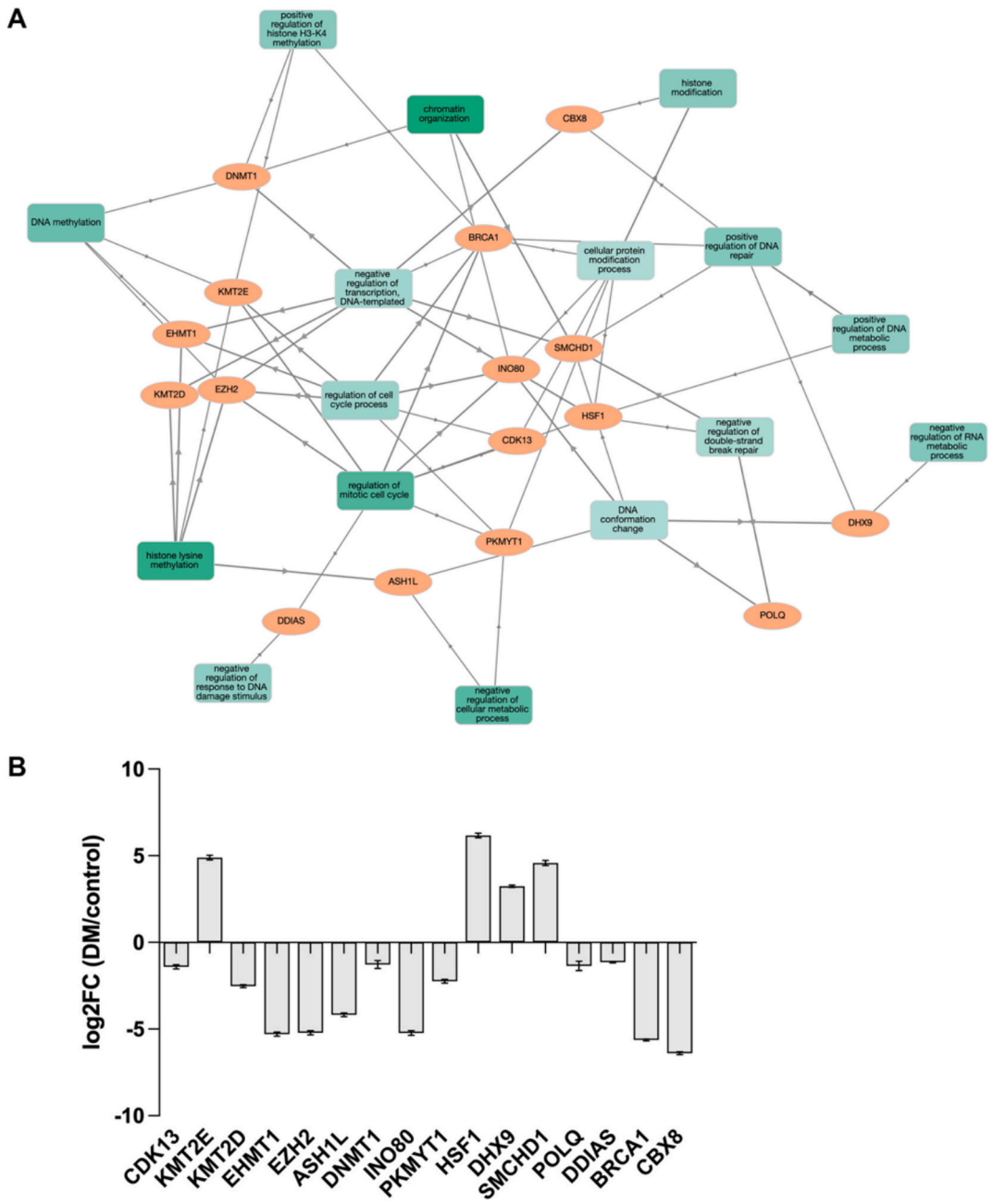


**Fig. 5.** Proteins marker related to cell cycle regulation and DNA damage responses (DDR). **(A)** GO enrichment network of genes significantly altered after 48-h DM treatment was generated using GOnet. Orange ellipses represent genes identified in the dataset, while green rectangles denote significantly enriched GO terms, including cell cycle regulation (GO:0051726), DNA repair (GO:0006281), response to DNA damage stimulus (GO:0006974), histone lysine methylation (GO:0034968), and chromatin organization (GO:0006325). Edges denote associations between genes and their enriched GO terms. **(B)** Differential protein expression levels ($log_2FC$) significantly different between DM-treated and control groups were calculated from the LFQ values performed in three independent experiments. (For interpretation of the references to colour in this figure legend, the reader is referred to the web version of this article.)

and the onset of cellular senescence. Furthermore, the proteins regulating DNA damage response (DDR) including HSF1 ($log_2FC$, 6.16), DHX9 ($log_2FC$, 3.24) and SMCHD1 ($log_2FC$, 4.58) were substantially increased in DM-treated cells (Fig. 5B). In contrast, the proteins involved in DNA repair mechanism and genome integrity including POLQ ($log_2FC$, −1.35), DDIAS ($log_2FC$, −1.13), BRCA1 ($log_2FC$, −5.63) and CBX8 ($log_2FC$, −6.40) were downregulated by DM treatment (Fig. 5B). Overall, DM exposure induced cells to express protein markers involved in DDR, cell cycle arrest and senescence.

### 3.4. Dimethoate induces early-stage apoptosis in SH-SY5Y cells

To determine whether DM induces apoptosis, we performed a flow cytometry-based assay to quantify cells that actively underwent apoptosis. Previously, CYP treatment has been reported to cause cell death via apoptotic processes (Promthep et al., 2022), and thus, CYP-treated cells were used as a positive control (Figs. 6A and B). Our results showed that DM treatment significantly increased the proportion of cells in early-stage apoptosis, but not in late-stage apoptosis, compared to the control group (Figs. 6A and B). Interestingly, DM exposure also resulted in a notable increase in Bcl-2, an anti-apoptotic protein (Fig. 6C). This suggests that DM-treated cells may develop resistance to

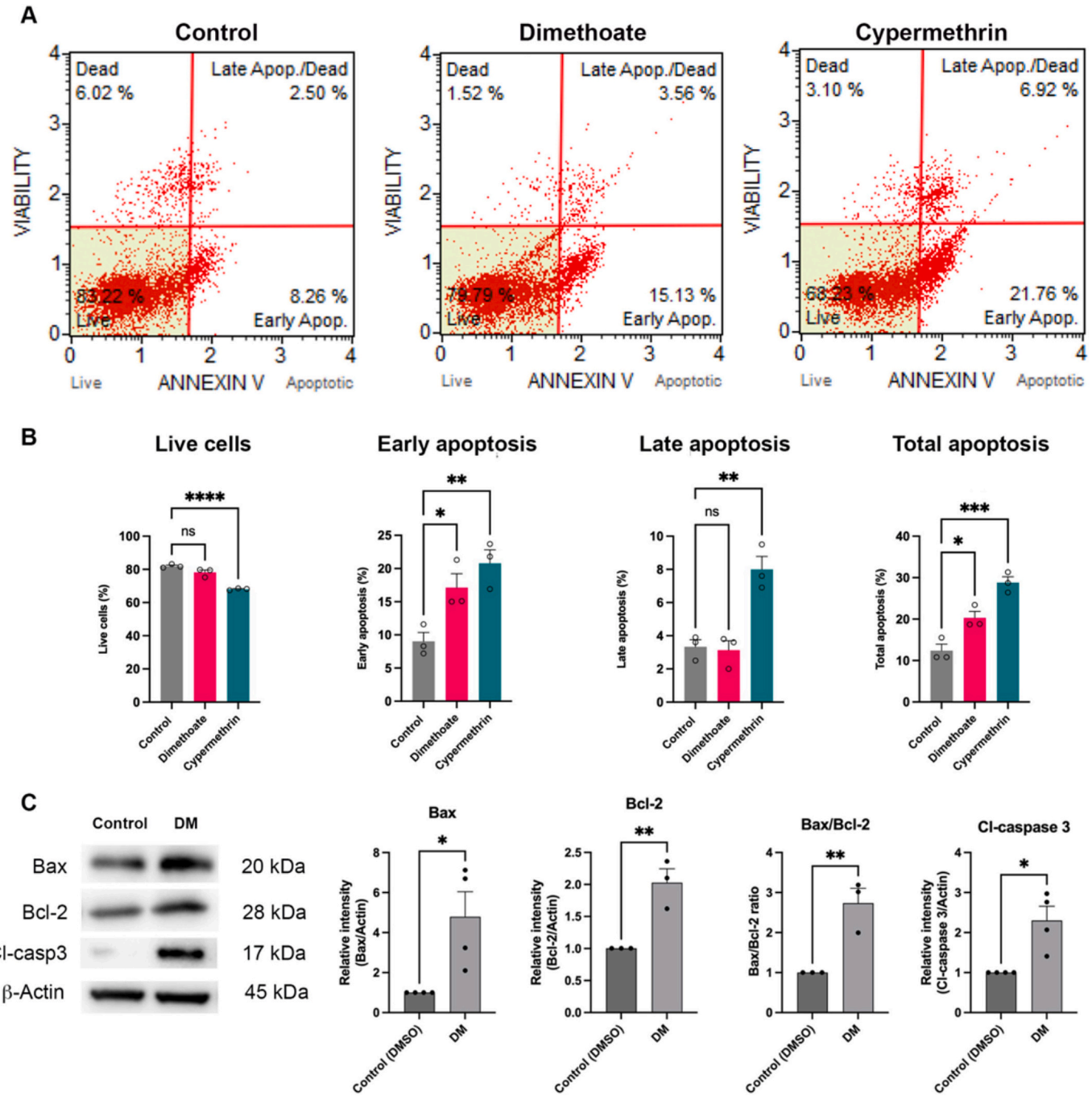


**Fig. 6.** Effect of DM treatment on cell death and apoptotic markers **(A)** The apoptotic profiles of control cells, 100 μM CYP-treated cells, and 100 μM DM-treated cells after 48 h of treatment are shown. **(B)** Percentages of live cells, early apoptosis, late apoptosis and total apoptosis are shown. **(C)** Effects of DM treatment on Bax, Bcl-2 and Cl-caspase 3 protein expressions were analyzed by Western blot. Data are presented as mean ± SEM, and significance is denoted as $*p < 0.05$, $*** p < 0.001$ and $**** p < 0.0001$ compared to the control group.

apoptosis, potentially shifting toward a senescent phenotype. Despite the upregulation of Bcl-2, the Bax/Bcl-2 ratio was significantly elevated, indicating the activation of pro-apoptotic signaling (Fig. 6C). In addition, the cleaved caspase-3 levels were increased in DM-treated cells, further supporting the initiation of apoptotic pathways, even though progression to late-stage apoptosis was not observed.

### 3.5. *DM treatment altered protein expressions of energy-sensing mediators*

Given that DM treatment reduced ATP levels (Fig. 3), suggesting metabolic stress, we hypothesized that nutrient-sensing mechanisms might be activated as a compensatory response. To investigate this, a targeted label-free nano-LC QTOF analysis using SWATH was employed to identify and quantify proteins involved in cellular responses to nutrient levels. Six proteins of interest–PRKAB1, RPTOR, MTOR, SIRT1, BECN1, and RHEB–were assessed. Consistent with ATP depletion, 5'-AMP-activated protein kinase (AMPK) subunit beta-1 (PPKAB1) was significantly upregulated, indicating activation of the AMPK signaling pathway (Figs. 7A and B). This increase was accompanied by elevated Beclin-1 (BECN1) levels, a key regulator of autophagy typically upregulated in response to energy stress. (Figs. 7A and B). However, no significant changes were detected in the protein expression of RPTOR,

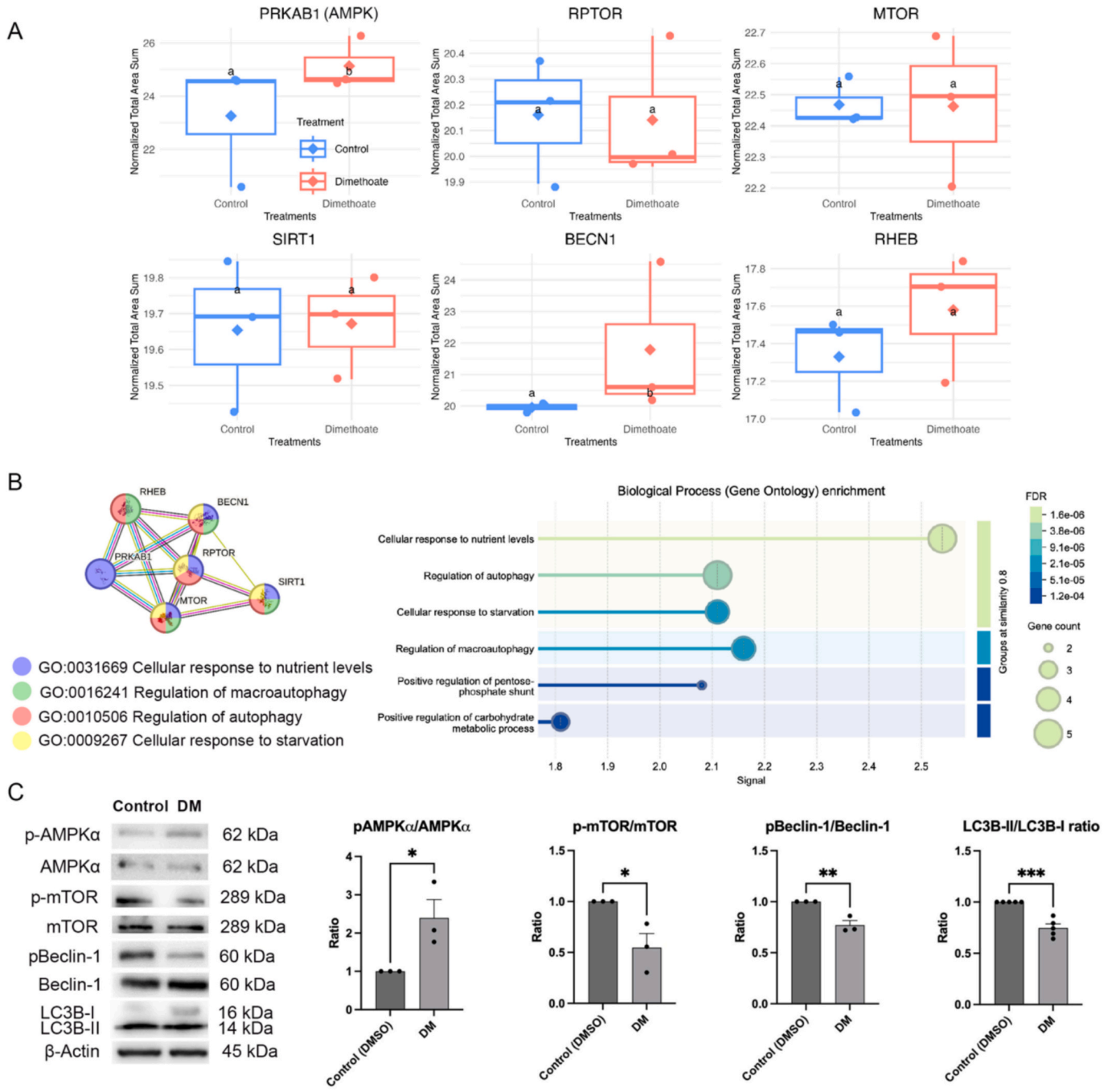


**Fig. 7.** DM treatment affects protein expressions in energy-sensing pathways. **(A)** A targeted label-free nano-LC QTOF analysis using SWATH. Letters "a" and "b" show statistical differences at $p < 0.001$ compared to the control group. A diamond shape marks the "mean" on the box plot. **(B)** Protein-protein interactions and functional enrichment (GO term analysis) were determined using the STRING database. Edge colors represent interaction sources: blue (co-occurrence), black (co-expression), purple (experimental evidence), light green (text mining), and light blue (curated databases). **(C)** Effects of DM treatment on protein levels of AMPK, mTOR, Beclin-1 and LC3B were analyzed by Western blot. (For interpretation of the references to colour in this figure legend, the reader is referred to the web version of this article.)

MTOR, SIRT1, and RHEB in DM-treated cells.

To validate these finding, Western blot analysis was performed. Although phosphorylated AMPK (p-AMPK) levels were elevated, the expression of downstream autophagy-related markers including phosphorylated mTOR (p-mTOR), p-Beclin-1, and the LC3-II/I ratio were significantly reduced (Fig. 7C), indicating a suppression of autophagic activity.

Collectively, these results suggest that while DM-induced ATP depletion activates AMPK signaling, it does not fully engage the downstream autophagy machinery. This incomplete adaptive response, in conjunction with mitochondrial dysfunction, early apoptosis, and senescence-related changes, may contribute to heightened neuronal vulnerability under DM exposure.

## 4. Discussion

DM exerts its primary toxic effects by inhibiting AChE, leading to excessive accumulation of acetylcholine at synapses and neuromuscular junctions (Fukuto, 1990). This overstimulates cholinergic signaling and results in neurotoxicity (Tarbah et al., 2007). However, emerging

evidence indicates that organophosphates may also target other cellular processes, including mitochondrial function, especially under chronic or sublethal exposure conditions (Nazam et al., 2020; Chen et al., 2017; Leung and Meyer, 2019). Mitochondria have been hypothesized to be another molecular target of organophosphates, due to their diverse adverse outcomes observed from chronic exposures (Leung and Meyer, 2019). Previously, DM and chlorpyrifos, another organophosphate, have been reported to cause mitochondrial fragmentation, mitochondrial membrane depolarization, and reduced intracellular levels of ATP (Nazam et al., 2020; Chen et al., 2017).

Here, we found that several mitochondria proteins including COX6A1, MT-ATP6 and TK2 were decreased by DM treatment, without affecting overall cell viability at sublethal concentrations (Fig. 1C). These proteins are critical for ATP production through oxidative phosphorylation (Figs. 2A–C). Specifically, mtATP6 encoding the F0 portion of ATP synthase subunits is responsible for the proton channel function to transfer the proton back into the matrix (Jonckheere et al., 2012). Consistently, DM exposure led to decreased oxygen consumption rates, reduced basal and maximal respiration, and impaired ATP production (Figs. 3A–D). Moreover, mitochondrial membrane depolarization and elevated superoxide levels were observed (Figs. 3G–J), markers commonly associated with ATP depletion, apoptotic signaling and oxidative stress (Guo et al., 2013; Tiwari et al., 2002).

Given that mitochondrial dysfunction and energy depletion are established triggers of cellular senescence (Miwa et al., 2022), we next examined whether DM exposure could induce a senescence-like state. Our results showed elevated p38 MAPK activation, increased p21 expression, and higher SA-β-gal activity (Figs. 4A and B), indicating a senescence-like phenotype. The activation of p38 MAPK has been demonstrated to mediate the induction of p21 and promote cellular senescence induced by $H_2O_2$ in human fibroblasts and melanocytes (Hou et al., 2022; Luo et al., 2011). p21 acts as a cell cycle inhibitor when localized in the nucleus, while the cytoplasmic p21 exhibits an anti-apoptotic effect upon phosphorylation (Ping et al., 2006). Activation of p21 has been reported in a p53-independent manner (Fang et al., 1999; Wang et al., 1999) and protects cells from the cytotoxic effects of radiation and toxic substances (Jung et al., 2010; Poluha et al., 1996). The activation of p21 commits the cell to growth arrest, which occurs through the binding of p21 to CDK4/6 to inactivate it. As a result, Rb remains bound to the transcriptional factor E2F1, preventing the cell cycle from progressing to the S phase. Senescence cells were reported to be resistant to cellular apoptosis, partly due to low expression level of p53 and the upregulation of anti-apoptotic protein Bcl-2 (Childs et al., 2014; Sanders et al., 2013).

Consistent with a senescence-prone state, DM treatment also led to downregulation of several epigenetic regulators that promote cell cycle progression, including KMT2D, EHMT1, EZH2, ASH1L and DNMT1 (Figs. 5A and B). Depletions of these proteins have been associated with cell cycle arrest, senescence and apoptosis (Ito et al., 2018; Lee et al., 2021; Lv et al., 2019; Yu et al., 2022). DM also suppressed the expression of INO80 and PKMYT1, the negative regulator of mitotic entry (Nakajima et al., 2008). The deficiency in these proteins caused defects in genome integrity and DNA damage (Nakajima et al., 2008; Hur et al., 2010). In addition, DM exposure dramatically increased the levels of proteins related to DNA damage signaling including HSF1, DHX9 and SMCHD1 (Vančevska et al., 2020; Fujimoto et al., 2017; Chakraborty and Hiom, 2021). On the contrary, the proteins related to DNA damage responses including POLQ, DDIAS, BRCA1 and CBX8 were down-regulated by DM treatment (Fig. 5B). Previous studies showed that dysregulations of these proteins resulted in sensitivity to genotoxic stresses, genome instability and cell death (Yousefzadeh and Wood, 2013; Wang et al., 2013; Won et al., 2017; Suberbielle et al., 2015; Oza et al., 2016).

Interestingly, despite signs of early apoptotic signaling, DM-treated cells resisted late-stage apoptosis (Figs. 6A and B). Markers of apoptosis initiation, such as Bax, cleaved caspase-3, and an elevated Bax/Bcl-2 ratio, were upregulated. However, execution of apoptosis was incomplete, suggesting a block in downstream apoptotic processes. The concurrent increase in Bcl-2 expression may represent a compensatory anti-apoptotic mechanism, helping cells resist cell death under metabolic stress (Fig. 6C). This balance between pro- and anti-apoptotic signaling likely contributes to a shift toward senescence, a state frequently observed under chronic stress conditions and characterized by metabolic dysfunction and cell cycle arrest.

We also found evidence of impaired autophagic responses in DM-treated cells (Fig. 7A and C). These findings suggest that adaptive mechanisms, such as AMPK activation and mTOR inhibition are engaged to counteract DM-induced energy depletion. Normally, energy stress activates AMPK and inhibits mTOR, promoting autophagy as a cyto-protective mechanism. In our study, DM exposure led to AMPK activation and mTOR inhibition, yet autophagy markers such as phosphorylated Beclin-1 and LC3-II/I ratios were reduced (Fig. 7C), indicating impaired autophagic flux. This insufficient autophagy may exacerbate cellular vulnerability by limiting the cell's ability to clear damaged organelles and proteins. One possible explanation is that DM disrupts the interplay between p38 MAPK and mTOR pathways, both of which are central regulators of the stress response. Such interference could blunt the protective benefits of autophagy and reinforce the shift toward senescence.

## 5. Conclusions

DM exposure did not induce cell death but led to cell cycle exit, senescence, and compromised energy production (Fig. 8). We demonstrate that DM impairs oxidative phosphorylation by downregulating key mitochondrial proteins and reducing ATP production, leading to metabolic stress. This stress response triggers early apoptotic signaling and oxidative damage, but instead of progressing to apoptosis, cells exhibit features of senescence, including p38 MAPK activation, p21 upregulation, and increased SA-β-gal activity. Notably, DM-treated cells show resistance to late-stage apoptosis and downregulation of critical epigenetic and DNA repair regulators, suggesting a compromised capacity for genome maintenance. Furthermore, although AMPK activation and mTOR inhibition are engaged as adaptive responses, impaired autophagic flux may exacerbate cellular vulnerability and reinforce the

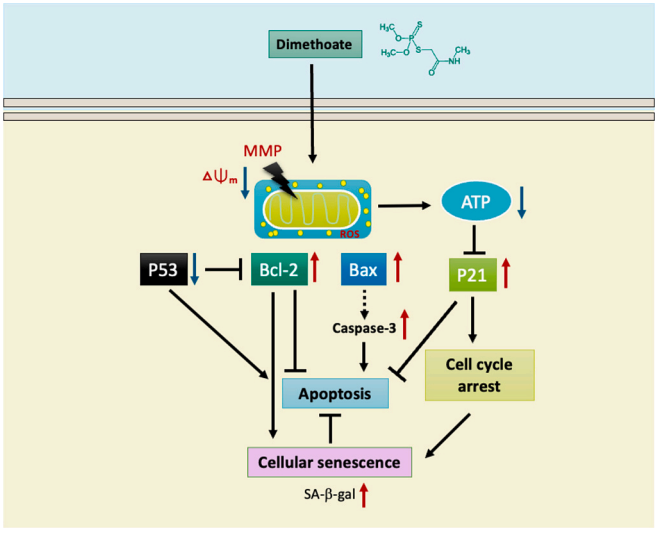


**Fig. 8.** DM exposure induces a senescence-like state in SH-SY5Y cells. SH-SY5Y cells treated with 100 μM DM for 48 h exhibit hallmarks of senescence, including upregulation of p21 and increased SA-β-gal activity, accompanied by a G0/G1 cell cycle arrest. DM exposure triggered p53-independent p21 activation, and apoptosis resistance was observed through elevated Bcl-2 expression.

senescence-like state. These results highlight the long-term consequences of DM on cellular metabolism and aging, with implications for neurotoxicity and aging-related pathologies. Given these potential impacts on cellular health, particularly in neuronal cells, this study suggests the need for heightened monitoring of dimethoate levels in environments. Reduced use and strict regulation of DM in agricultural and industrial settings may help to minimize these long-term health risks. Public awareness and ongoing assessment of exposure limits could further contribute to safeguarding against its harmful effects, particularly for vulnerable populations.

## CRediT authorship contribution statement

**Phorutai Pearngam:** Writing – review & editing, Writing – original draft, Visualization, Methodology, Investigation, Formal analysis, Conceptualization. **Kornkanok Promthep:** Visualization, Methodology, Investigation, Formal analysis. **Tanya Prasertporn:** Methodology, Investigation, Formal analysis. **Kittikun Songsomboon:** Writing – original draft, Investigation, Formal analysis. **Tanthai Polvat:** Formal analysis. **Jiratchaya Charoenkul:** Investigation, Formal analysis. **Sujira Mukda:** Writing – review & editing, Supervision, Resources, Methodology. **Piyarat Govitrapong:** Writing – review & editing, Supervision, Resources, Methodology. **Chutikorn Nopparat:** Writing – review & editing, Writing – original draft, Visualization, Supervision, Methodology, Investigation, Formal analysis, Conceptualization. **Jiraporn Panmanee:** Writing – review & editing, Writing – original draft, Visualization, Methodology, Investigation, Funding acquisition, Formal analysis, Conceptualization.

## Declaration of competing interest

The authors declare no conflict of interest regarding the publication of this study.

## Acknowledgement

This research project is supported by Mahidol University (Strategic Research Fund): fiscal year 2023 to JP (grant number MU-SRF-ST-01 A/66). We would like to thank MUAI Center, Faculty of Information and Communication Technology, Mahidol University, Thailand for supporting computer facility. We thank Pattanai Konpetch from Department of Biomedical Sciences, College of Integrated Health Sciences, University at Albany, Albany, NY, USA for his contribution to the scientific illustration in the summary figure. Finally, we thank Chonticha Subkod and Patlada Tangweerasing for their valuable assistance with the Western blotting experiments.

## Data availability

Data will be made available on request.

## References

Aly, N.M., El-Gendy, K.S., 2000. Effect of dimethoate on the immune system of female mice. J. Environ. Sci. Health B 35, 77–86.
Astiz, M., Diz-Chaves, Y., Garcia-Segura, L.M., 2013. Sub-chronic exposure to the insecticide dimethoate induces a proinflammatory status and enhances the neuroinflammatory response to bacterial lypopolysaccharide in the hippocampus and striatum of male mice. Toxicol. Appl. Pharmacol. 272, 263–271.
Ben Amara, I., Karray, A., Hakim, A., Ben Ali, Y., Troudi, A., Soudani, N., Boudawara, T., Zeghal, K.M., Zeghal, N., 2013. Dimethoate induces kidney dysfunction, disrupts membrane-bound ATPases and confers cytotoxicity through DNA damage. Protective effects of vitamin E and selenium. Biol. Trace Elem. Res. 156, 230–242.
Chakraborty, P., Hiom, K., 2021. DHX9-dependent recruitment of BRCA1 to RNA promotes DNA end resection in homologous recombination. Nat. Commun. 12, 4126.
Chen, T., Tan, J., Wan, Z., Zou, Y., Afewerky, H.K., Zhang, Z., Zhang, T., 2017. Effects of commonly used pesticides in China on the mitochondria and ubiquitin-proteasome system in Parkinson's disease. Int. J. Mol. Sci. 18.
Childs, B.G., Baker, D.J., Kirkland, J.L., Campisi, J., van Deursen, J.M., 2014. Senescence and apoptosis: dueling or complementary cell fates? EMBO Rep. 15, 1139–1153.
Correia-Melo, C., Marques, F.D., Anderson, R., Hewitt, G., Hewitt, R., Cole, J., Carroll, B. M., Miwa, S., Birch, J., Merz, A., Rushton, M.D., Charles, M., Jurk, D., Tait, S.W., Czapiewski, R., Greaves, L., Nelson, G., Bohlooly, Y.M., Rodriguez-Cuenca, S., Vidal-Puig, A., Mann, D., Saretzki, G., Quarato, G., Green, D.R., Adams, P.D., von Zglinicki, T., Korolchuk, V.I., Passos, J.F., 2016. Mitochondria are required for pro-ageing features of the senescent phenotype. EMBO J. 35, 724–742.
de Andrade, A.R.B., de Carvalho, D.L., Kishishita, J., Pimenta, C.A.P., Souza, A.T.M., de Santana, D.P., Leal, L.B., 2022. Dimethoate absorption: a complementary in vitro and in vivo assessment. Environ. Toxicol. Pharmacol. 95, 103961.
Fang, L., Igarashi, M., Leung, J., Sugrue, M.M., Lee, S.W., Aaronson, S.A., 1999. p21Waf1/Cip1/Sdi1 induces permanent growth arrest with markers of replicative senescence in human tumor cells lacking functional p53. Oncogene 18, 2789–2797.
Fujimoto, M., Takii, R., Takaki, E., Katiyar, A., Nakato, R., Shirahige, K., Nakai, A., 2017. The HSF1–PARP13–PARP1 complex facilitates DNA repair and promotes mammary tumorigenesis. Nat. Commun. 8, 1638.
Fukuto, T.R., 1990. Mechanism of action of organophosphorus and carbamate insecticides. Environ. Health Perspect. 87, 245–254.
Guo, C., Sun, L., Chen, X., Zhang, D., 2013. Oxidative stress, mitochondrial damage and neurodegenerative diseases. Neural Regen. Res. 8, 2003–2014.
Hou, X., Shi, J., Sun, L., Song, L., Zhao, W., Xiong, X., Lu, Y., 2022. The involvement of ERK1/2 and p38 MAPK in the premature senescence of melanocytes induced by H(2)O(2) through a p53-independent p21 pathway. J. Dermatol. Sci. 105, 88–97.
Hur, S.K., Park, E.J., Han, J.E., Kim, Y.A., Kim, J.D., Kang, D., Kwon, J., 2010. Roles of human INO80 chromatin remodeling enzyme in DNA replication and chromosome segregation suppress genome instability. Cell. Mol. Life Sci. 67, 2283–2296.
Ito, T., Teo, Y.V., Evans, S.A., Neretti, N., Sedivy, J.M., 2018. Regulation of cellular senescence by Polycomb chromatin modifiers through distinct DNA damage- and histone methylation-dependent pathways. Cell Rep. 22, 3480–3492.
Jonckheere, A.I., Smeitink, J.A., Rodenburg, R.J., 2012. Mitochondrial ATP synthase: architecture, function and pathology. J. Inherit. Metab. Dis. 35, 211–225.
Jung, Y.S., Qian, Y., Chen, X., 2010. Examination of the expanding pathways for the regulation of p21 expression and activity. Cell. Signal. 22, 1003–1012.
Kim, J.H., Kang, J.C., 2015. Oxidative stress, neurotoxicity, and non-specific immune responses in juvenile red sea bream, *Pagrus major*, exposed to different waterborne selenium concentrations. Chemosphere 135, 46–52.
Lee, J., Kim, K., Ryu, T.Y., Jung, C.R., Lee, M.S., Lim, J.H., Park, K., Kim, D.S., Son, M.Y., Hamamoto, R., Cho, H.S., 2021. EHMT1 knockdown induces apoptosis and cell cycle arrest in lung cancer cells by increasing CDKN1A expression. Mol. Oncol. 15, 2989–3002.
Leung, M.C.K., Meyer, J.N., 2019. Mitochondria as a target of organophosphate and carbamate pesticides: revisiting common mechanisms of action with new approach methodologies. Reprod. Toxicol. 89, 83–92.
Luo, Y., Zou, P., Zou, J., Wang, J., Zhou, D., Liu, L., 2011. Autophagy regulates ROS-induced cellular senescence via p21 in a p38 MAPKα dependent manner. Exp. Gerontol. 46, 860–867.
Lv, S., Wen, H., Shan, X., Li, J., Wu, Y., Yu, X., Huang, W., Wei, Q., 2019. Loss of KMT2D induces prostate cancer ROS-mediated DNA damage by suppressing the enhancer activity and DNA binding of antioxidant transcription factor FOXO3. Epigenetics 14, 1194–1208.
Martínez-Morcillo, S., Pérez-López, M., Soler-Rodríguez, F., González, A., 2019. The organophosphorus pesticide dimethoate decreases cell viability and induces changes in different biochemical parameters of rat pancreatic stellate cells. Toxicol. in Vitro 54, 89–97.
Miwa, S., Kashyap, S., Chini, E., von Zglinicki, T., 2022. Mitochondrial dysfunction in cell senescence and aging. J. Clin. Invest. 132.
Na Nakorn, P., Pannengpetch, S., Isarankura-Na-Ayudhya, P., Thippakorn, C., Lawung, R., Sathirapongsasuti, N., Kitiyakara, C., Sritara, P., Vathesatogkit, P., Isarankura-Na-Ayudhya, C., 2020. Roles of kininogen-1, basement membrane specific heparan sulfate proteoglycan core protein, and roundabout homolog 4 as potential urinary protein biomarkers in diabetic nephropathy. EXCLI J. 19, 872–891.
Nakajima, H., Yonemura, S., Murata, M., Nakamura, N., Piwnica-Worms, H., Nishida, E., 2008. Myt1 protein kinase is essential for Golgi and ER assembly during mitotic exit. J. Cell Biol. 181, 89–103.
Nazam, N., Lone, M.I., Hamid, A., Qadah, T., Banjar, A., Alam, Q., Saeed, M., Ahmad, W., 2020. Dimethoate induces DNA damage and mitochondrial dysfunction triggering apoptosis in rat bone-marrow and peripheral blood cells. Toxics 8.
Oza, J., Ganguly, B., Kulkarni, A., Ginjala, V., Yao, M., Ganesan, S., 2016. A novel role of Chromodomain protein CBX8 in DNA damage response. J. Biol. Chem. 291, 22881–22893.
Panmanee, J., Phanchana, M., Pearngam, P., Petchyam, N., Promthep, K., Wisomka, P., Kutpruek, S., Pannengpetch, S., Prasertporn, T., Mukda, S., Govitrapong, P., Nopparat, C., 2025. A proteomics profiling reveals the neuroprotective effects of melatonin on exogenous β-amyloid-42 induced mitochondrial impairment, intracellular β-amyloid accumulation and tau hyperphosphorylation in human SH-SY5Y cells. Cell Biol. Int. 49 (6), 659–673.
Ping, B., He, X., Xia, W., Lee, D.F., Wei, Y., Yu, D., Mills, G., Shi, D., Hung, M.C., 2006. Cytoplasmic expression of p21CIP1/WAF1 is correlated with IKKbeta overexpression in human breast cancers. Int. J. Oncol. 29, 1103–1110.
Poluha, W., Poluha, D.K., Chang, B., Crosbie, N.E., Schonhoff, C.M., Kilpatrick, D.L., Ross, A.H., 1996. The cyclin-dependent kinase inhibitor p21 (WAF1) is required for survival of differentiating neuroblastoma cells. Mol. Cell. Biol. 16, 1335–1341.
Pomaznoy, M., Ha, B., Peters, B., 2018. GOnet: a tool for interactive gene ontology analysis. BMC Bioinformatics 19, 470.

Promthep, K., Nopparat, C., Mukda, S., Pannengpetch, S., Wisomka, P., Chantadul, V., Phanchana, M., Panmanee, J., 2022. Proteomic profiling reveals neuronal ion channel dysregulation and cellular responses to DNA damage-induced cell cycle arrest and senescence in human neuroblastoma SH-SY5Y cells exposed to cypermethrin. Neurotoxicology 93, 71–83.
R.C. Team, 2014. R: a language and environment for statistical computing. MSOR Connect. 1.
Ritchie, M.E., Phipson, B., Wu, D., Hu, Y., Law, C.W., Shi, W., Smyth, G.K., 2015. Limma powers differential expression analyses for RNA-sequencing and microarray studies. Nucleic Acids Res. 43, e47.
Russell, L., 2018. Emmeans: Estimated Marginal Means, Aka Least-Squares Means, R Package Version, 1.
Sagar, N.A., Pareek, S., Sharma, S., Yahia, E.M., Lobo, M.G., 2018. Fruit and vegetable waste: bioactive compounds, their extraction, and possible utilization. Compr. Rev. Food Sci. Food Saf. 17, 512–531.
Sanders, Y.Y., Liu, H., Zhang, X., Hecker, L., Bernard, K., Desai, L., Liu, G., Thannickal, V. J., 2013. Histone modifications in senescence-associated resistance to apoptosis by oxidative stress. Redox Biol. 1, 8–16.
Sang, C., Yu, Z., An, W., Borgen Sørensen, P., Jin, F., Yang, M., 2022. Development of a data driven model to screen the priority control pesticides in drinking water based on health risk ranking and contribution rates. Environ. Int. 158, 106901.
Sharma, Y., Bashir, S., Irshad, M., Nag, T.C., Dogra, T.D., 2005. Dimethoate-induced effects on antioxidant status of liver and brain of rats following subchronic exposure. Toxicology 215, 173–181.
Suberbielle, E., Djukic, B., Evans, M., Kim, D.H., Taneja, P., Wang, X., Finucane, M., Knox, J., Ho, K., Devidze, N., Masliah, E., Mucke, L., 2015. DNA repair factor BRCA1 depletion occurs in Alzheimer brains and impairs cognitive function in mice. Nat. Commun. 6, 8897.
Tarbah, F.A., Shaheen, A.M., Benomran, F.A., Hassan, A.I., Daldrup, T., 2007. Distribution of dimethoate in the body after a fatal organophosphate intoxication. Forensic Sci. Int. 170, 129–132.
Tiwari, B.S., Belenghi, B., Levine, A., 2002. Oxidative stress increased respiration and generation of reactive oxygen species, resulting in ATP depletion, opening of mitochondrial permeability transition, and programmed cell death. Plant Physiol. 128, 1271–1281.
Van Scoy, A., Pennell, A., Zhang, X., 2016. Environmental fate and toxicology of Dimethoate. Rev. Environ. Contam. Toxicol. 237, 53–70.
Vančevska, A., Ahmed, W., Pfeiffer, V., Feretzaki, M., Boulton, S.J., Lingner, J., 2020. SMCHD1 promotes ATM-dependent DNA damage signaling and repair of uncapped telomeres. EMBO J. 39, e102668.
Walsh, L.P., Webster, D.R., Stocco, D.M., 2000. Dimethoate inhibits steroidogenesis by disrupting transcription of the steroidogenic acute regulatory (StAR) gene. J. Endocrinol. 167, 253–263.
Wang, Y., Blandino, G., Givol, D., 1999. Induced p21waf expression in H1299 cell line promotes cell senescence and protects against cytotoxic effect of radiation and doxorubicin. Oncogene 18, 2643–2649.
Wang, J., He, J., Su, F., Ding, N., Hu, W., Yao, B., Wang, W., Zhou, G., 2013. Repression of ATR pathway by miR-185 enhances radiation-induced apoptosis and proliferation inhibition. Cell Death Dis. 4, e699.
Wang, X., Sui, X., Sun, Y., Cui, Z., Ma, N., Wang, S., Yang, J., Liu, F., Yang, W., Xiao, Z., Zhu, T., Luo, Y., Wang, Y., 2024. Potential common mechanisms of cytotoxicity induced by organophosphorus pesticides via NLRP3 Inflammasome activation. Geohealth 8, e2023GH000888.
Wiley, C.D., Campisi, J., 2021. The metabolic roots of senescence: mechanisms and opportunities for intervention. Nat. Metab. 3, 1290–1301.
Won, K.J., Im, J.Y., Kim, B.K., Ban, H.S., Jung, Y.J., Jung, K.E., Won, M., 2017. Stability of the cancer target DDIAS is regulated by the CHIP/HSP70 pathway in lung cancer cells. Cell Death Dis. 8, e2554.
Yousefzadeh, M.J., Wood, R.D., 2013. DNA polymerase POLQ and cellular defense against DNA damage. DNA Repair (Amst) 12, 1–9.
Yu, M., Jia, Y., Ma, Z., Ji, D., Wang, C., Liang, Y., Zhang, Q., Yi, H., Zeng, L., 2022. Structural insight into ASH1L PHD finger recognizing methylated histone H3K4 and promoting cell growth in prostate cancer. Front. Oncol. 12, 906807.
Zhou, L., Chen, X., Liu, T., Gong, Y., Chen, S., Pan, G., Cui, W., Luo, Z.P., Pei, M., Yang, H., He, F., 2015. Melatonin reverses H2 O2 -induced premature senescence in mesenchymal stem cells via the SIRT1-dependent pathway. J. Pineal Res. 59, 190–205.